PHYSICAL REVIEW D **94,** 053014 (2016)

Boosting invisible searches via ZH: From the Higgs boson to dark matter simplified models

Dorival Gonçalves,[1] Frank Krauss,[1] Silvan Kuttimalai,[1] and Philipp Maierhöfer[2]

[1]*Institute for Particle Physics Phenomenology, Physics Department, Durham University, Durham DH1 3LE, United Kingdom*

[2]*Physikalisches Institut, Albert-Ludwigs-Universität Freiburg, 79104 Freiburg, Germany*

(Received 7 June 2016; published 28 September 2016)

Higgs boson production in association with a Z boson at the LHC is analyzed, both in the Standard Model and in simplified model extensions for dark matter. We focus on $H \to$ invisibles searches and show that loop-induced components for both the signal and background present phenomenologically relevant contributions to the $\mathcal{BR}(H \to \text{inv})$ limits. We also show how multijet merging improves the description of key distributions to this analysis. In addition, the constraining power of this channel to simplified models for dark matter with scalar and pseudoscalar mediators ϕ and A is discussed and compared with noncollider constraints. We find that with 100 fb^{-1} of LHC data, this channel provides competitive constraints to the noncollider bounds, for most of the parameter space we consider, bounding the universal Standard Model fermion-mediator strength at $g_v < 1$ for moderate masses in the range of 100 GeV $< m_{\phi/A} <$ 400 GeV.

DOI: 10.1103/PhysRevD.94.053014

I. INTRODUCTION

Constraining the invisible decay width of the Higgs boson is a cornerstone of the LHC program [1–6]. The Standard Model (SM) predicts a very small Higgs to invisible decay width which is practically inaccessible with the LHC sensitivity. However, many models collectively referred to as Higgs portal models predict a larger invisible branching ratio [7,8]. The main hope of these models is to establish a link to a potential dark sector through the Higgs boson. Therefore, any determination of the invisible decay width of the Higgs boson would directly represent a new physics discovery and could be connected to a dark matter (DM) candidate.

One of the most prominent and phenomenologically stringent LHC invisible Higgs search channels is Higgs-strahlung, ZH production. The associated Z and Higgs boson production generates an interesting signature, characterised by a boosted dileptonic pair recoiling against large missing transverse energy. The current upper bounds derived with this channel by the LHC experiments are $\mathcal{BR}(H \to \text{inv}) < 0.75$ and 0.58 at 95% C.L. for ATLAS and CMS, respectively [3].

In this paper, the Higgs-strahlung channel is carefully explored, emphasizing the fundamental ingredients for a robust theoretical prediction. In particular, we show that both the loop-induced signal ZH and backgrounds WW and ZZ play a fundamental role. To our knowledge, this is the first dedicated study that scrutinizes the importance of the latter in the considered search. We also show their impact in a full signal-background study deriving the LHC $\mathcal{BR}(H \to \text{inv})$ limits. In addition, we show how multijet merging algorithms improve the description of key distributions for this analysis.

The present study is further extended to a set of simplified models for dark matter. In these models, DM is produced through a scalar ϕ or a pseudoscalar A mediator that produces relevant rates through the loop-induced $Z\phi(A)$ channel. We derive the LHC sensitivity as a function of the mediator mass.

This paper is organized as follows. In Sec. II, the importance of the loop-induced components to signal and background is quantified, and the importance of multijet merging techniques to the current Higgs-strahlung searches is discussed. In Sec. III, a complete signal-background analysis is presented for searches for invisible Higgs decays, and we derive the sensitivity of the current Run II at the LHC. In Sec. IV, we further extend this analysis, exploring the simplified models for dark matter via the $Z\phi(A)$ channel. The summary of our results is presented in Sec. V.

II. INGREDIENTS OF THE ANALYSIS

A. Loop-induced signal and background

The Higgs-strahlung signal $Z(ll)H(\text{inv})$ and dominant background $VV' = Z(ll)Z(\nu\nu), W(l\nu)W(l\nu)$ present structural similarities relevant for the invisible searches. Both are dominated, at the level of total rates, by the quark-initiated subprocesses, which we refer to as Drell-Yan (DY)-like, and indicate them with the subscript qq. In both cases, ZH and VV', there are also loop-induced gluon fusion (GF) contributions, indicated by the subscript gg, that become important in some kinematic regimes despite their subleading corrections to the total rate [9–17]. It is clear that this classification, strictly speaking is valid at Born level only; higher-order corrections of course also include

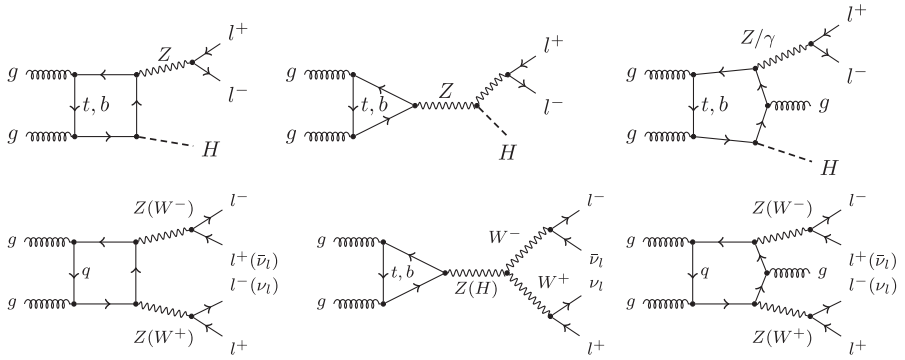

FIG. 1. Top panel: Representative loop-induced Feynman diagrams contributing to the signal $Z(ll)H$ (left and central) and $Z(ll)Hj$ (right). Bottom panel: The same for the background ZZ and WW (left and central) and ZZj, WWj (right). In the massless limit for first- and second-generation quarks, only top and bottom flavors contribute to the triangle graphs as a consequence of Furry's theorem.

different initial states. In addition, the loop-induced contributions are part of the next-to-next-to-leading-order correction to the process, which do not interfere with the other contributions at this order. However, current event simulation technology is not yet able to include these contributions in a more systematic way, and they have to be added as independent samples.[1] In Fig. 1, we display a representative sample of the GF Feynman diagrams for both signal and background.

Notably, there are two main requirements in the invisible searches that result in enriching these loop-induced contributions. First, the analysis usually accounts separately for the zero- and one-jet exclusive bins. This strategy is very efficient to suppress the initially overwhelming $t\bar{t}+$ jets background, especially in association with a b-tagging veto. Second, it requires large missing energy in the event selection, usually $\not{E}_T \gtrsim 100$ GeV. This selection in particular depletes the $Z(ll)+$ jets background [3]. Combining these two ingredients results in important phenomenological implications. They are illustrated in Fig. 2, where the missing energy distributions are displayed for the signal ZH and background VV' in the zero- (left) and one-jet (right) exclusive bins.

While the GF VV' background presents an almost flat contribution over the whole missing energy distribution, the ZH signal shows a phenomenologically relevant threshold at $\not{E}_T \sim m_t$. The GF signal is driven by the heavy flavor quark loops with their characteristic branch cut at $m_{ZH} \sim 2m_t$ resulting in relevant rates for the boosted regime. On the other hand, the GF background is dominated by light flavor quark corrections, without any such structure. The top-quark loop contribution, which in the GF background also presents a branch cut, enhances at the boosted regime as well. However, this is a subleading correction only when compared to the other five light flavor quark loops. Hence, no phenomenologically relevant enhancement is observed in this component at the boosted regime.

The GF signal presents relevant effects that can amount to ∼30% of the signal rate for the zero-jet bin, and up to ∼50% for the one-jet bin around the top mass threshold. The GF VV' background presents smaller contributions, entailing approximately ∼10% of its background rate for the zero-jet case and ∼15% for the one-jet case. The larger initial-state color factor for the GF leads to a higher radiation probability in comparison to the DY component. I.e., the zero-jet sample tends to be more populated by the DY component and the higher multiplicities receive larger contributions from the GF. Thus, robust predictions for both the signal and background samples have to account for the GF component. We note that the GF signal component also renders important contributions to the hadronic Higgs decay channel $ZH(b\bar{b})$. In particular, it leads to phenomenologically relevant modifications to the invariant mass distribution to the Higgs fat-jet. This phenomenological effect has direct impact for instance on the bottom Yukawa bounds. See Ref. [9] for more details.

B. Multijet merging

The separation of the signal and background in jet bins has become a common ingredient in many LHC analyses with complex backgrounds. For the invisible searches, as previously highlighted, this procedure is also customary since the initially overwhelming $t\bar{t}+$ jets background can be brought under control with jet vetoes.

The tool of choice to properly account for the detailed QCD emissions in each jet sample is multijet merging. Our simulation takes into account the following contributions. The Drell-Yan like signal $Z(ll)H$ and background $V^{(*)}V'^{(*)}$ are merged up to one jet at next-to-leading-order (NLO) precision through the MEPS@NLO algorithm [18], which can be understood as the combination of towers of MC@NLO simulations into one inclusive sample without double counting of extra emissions [19,20]. The respective loop-induced components are generated at leading

[1]Similarly to the Higgs pair production, higher-order QCD effects result in large corrections to the considered GF processes. The GF rates account for $K = 2$ [9,10].

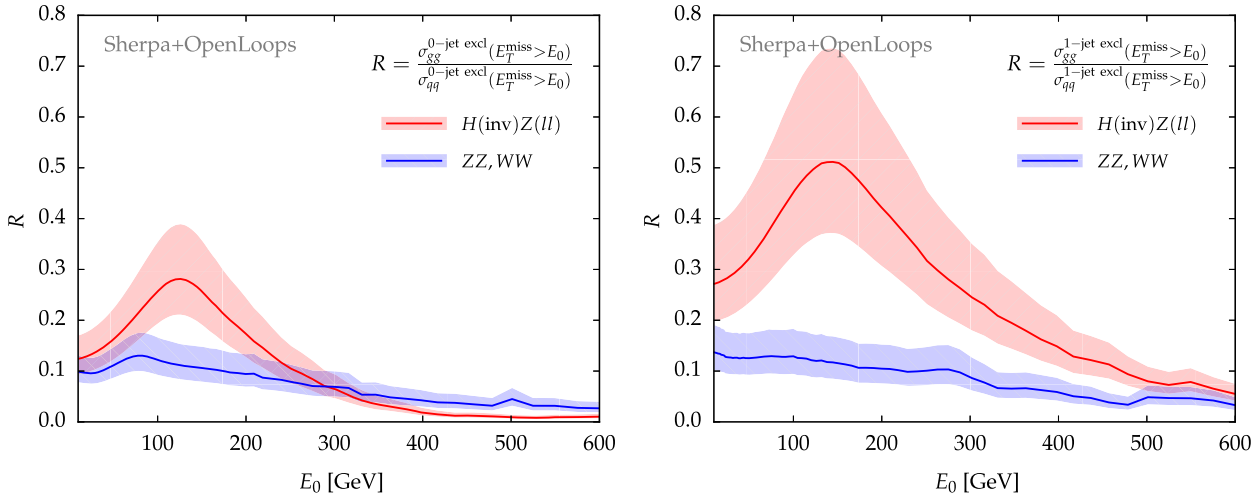

FIG. 2. The fraction of the gluon fusion contribution to the Higgs-strahlung cross section, for the $Z(ll)H(\text{inv})$ signal as well as the $V^{(*)}V'^{(*)} = Z(ll)Z(\nu\nu), W(l\nu)W(l\nu)$ background, as a function of the $E_T > E_0$ selection cut in the zero-jet (left panel) and one-jet (right panel) exclusive bins. Spin correlations and off-shell effects are fully accounted for in the vector-boson decays. The NLO Drell-Yan and the loop-induced gluon fusion samples, for signal and background, are merged up to one jet, at next-to-leading order and at leading order, respectively. The uncertainty bands result from three-point scale variations on the matrix element.

order (LO) and also merged up to one jet, denoted by MEPS@LOOP^2 [21].

In Fig. 3 (left) the missing energy distribution is displayed for the signal and VV' background components. We observe that they produce similar rates either for their DY (dashed) or GF (full) components at the phenomenologically relevant boosted kinematics regime. In the lower panel, the ratio of the multijet merged sample (MEPS@LOOP^2) to the naive LO plus parton shower (LOOP^2 + PS) GF samples is shown. The latter is the approach typically followed in current experimental studies for the signal predictions [3], where the GF jet emission is based only on the parton shower approximation. Although the background presents a flat correction profile, the signal

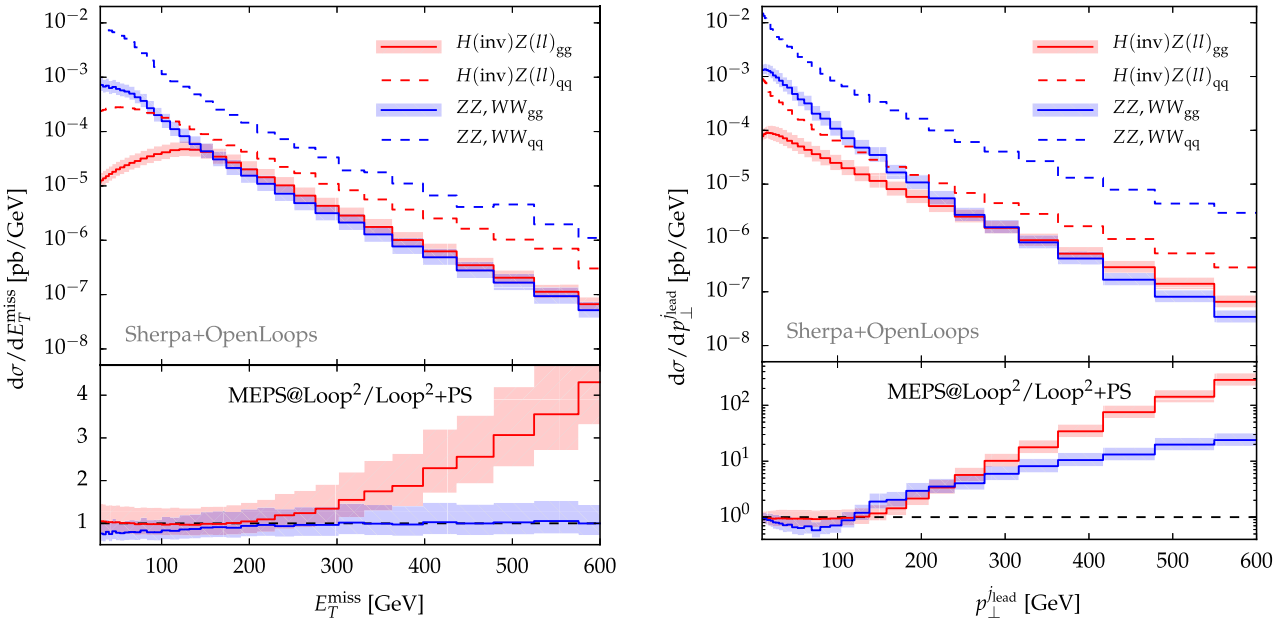

FIG. 3. Missing energy distribution E_T (left) and leading jet transverse momentum $p_T^{j_{\text{lead}}}$ distribution (right) for the signal $Z(ll)H(\text{inv})$ and background $W^{(*)}W^{(*)}, Z^{(*)}Z^{(*)}$ components assuming $\mathcal{BR}(H \to \text{inv}) = 1$. The signal and background are both decomposed in Drell-Yan-like and loop-induced components, which are generated by MEPS@NLO and MEPS@LOOP^2, with up to one-jet merged. The bottom panel displays the ratio between the merged sample and the pure LO (i.e., box only) plus parton shower loop-induced samples for both signal (red) and background (blue).

displays a major enhancement with the missing energy distribution for $\not{E}_T > m_t$ that can reach up to a factor of $\mathcal{O}(4)$ at $\not{E}_T \sim 600$ GeV [9]. This effect has a similar origin to the $H +$ jets top mass contributions at the boosted regime [22,23]. The missing transverse energy can obtain its recoil from jet emissions, which directly probe the loop structure. This loop factor is dominated by the top-quark mass effects in the signal case. If the $\not{E}_T$ exceeds the top mass threshold, the effects of the loops in the corresponding matrix elements become large. This feature is not captured in the $\text{LOOP}^2 + \text{PS}$ approximation where the jet is generated purely through an initial-state gluon splitting. Since it is fundamentally related to the top-quark contributions, the signal presents a large correction, while the background—which is predominantly generated by light quark loops—does not produce any appreciable change.

Merging effects are even larger when considering jet observables. Without merging, any extra parton-level QCD radiation is generated only by the parton shower and hard jets are, correspondingly, not appropriately described. In Fig. 3 (right), we present the transverse momentum distribution of the hardest jet for both signal and background contributions. Large discrepancies show up when comparing the spectra obtained from a $\text{LOOP}^2 + \text{PS}$-type simulation with the ones obtained from the corresponding merged samples. In the region of large transverse momenta, the $\text{LOOP}^2 + \text{PS}$ prediction underestimates the spectrum by orders of magnitude. For example, a relative factor of $\mathcal{O}(10)$ is observed for $p_T^{j_{\text{lead}}} \sim 300$ GeV which is even further enhanced at higher energies. In this regime, the soft/collinear approximation inherent to the parton shower fails. By merging matrix elements with one additional jet into the sample, we recover the corresponding fixed-order matrix element accuracy that is required for an appropriate description in this regime. The signal and background merging corrections present a similar pattern below the top threshold. Above this threshold, however, again large corrections for the signal sample are observed. This essentially recovers the results already present in Fig. 3 (left), where the effects in the signal sample where much larger than in the background for this regime.[2]

In conclusion, any robust theoretical description with the usual separation in jet bins and the boosted kinematics selections requires the inclusion of the loop-induced components and multijet merging algorithms, for both the signal and the background.

III. CONSTRAINTS ON INVISIBLE DECAYS

In this section, the constraining power of the Higgs-strahlung $Z(ll)H$ channel to the branching ratio of invisible decays of the Higgs boson, $\mathcal{BR}(H \to \text{inv})$ at the $\sqrt{s} = 13$ TeV LHC is analyzed. The major backgrounds for this process are diboson pair $V^{(*)}V'^{(*)} = WW, WZ, ZZ$, top pair $t\bar{t} +$ jets, and $Z +$ jets production.

The Monte Carlo studies in this paper are performed with SHERPA + OPENLOOPS [24–26]. The DY $Z(ll)H$, DY VV', $t\bar{t} +$ jets, and $Z +$ jets samples are generated with the MEPS@NLO algorithm [18], with up to one extra jet at NLO (QCD) accuracy for all processes apart from $Z +$ jets, where up to two jets have been treated at NLO. The loop-induced GF components are generated with the MEPS@LOOP^2 algorithm [21]. These samples are again merged up to one extra jet, this time at LO. Finite-width effects and spin correlations from the leptonic vector-boson decays are fully accounted for in the simulation. Hadronization and underlying event effects are also included.

In our event analysis, we require two isolated, same-flavor, opposite-sign leptons with $p_{Tl} > 20$ GeV and $|\eta_l| < 2.5$. The lepton isolation criterion demands less than 20% of hadronic activity in a radius of $R = 0.2$ around the lepton. The invariant mass of the dilepton system m_{ll} is required to fall into the Z-boson mass window $|m_{ll} - m_Z| < 15$ GeV. Jets are defined with the anti-k_T jet algorithm with radius $R = 0.4$, $p_{Tj} > 30$ GeV, and $|\eta_j| < 5$ using the FASTJET package [27]. To suppress the initially overwhelming $t\bar{t}$ background, b-tagged jets are vetoed, assuming a 70% b-tagging efficiency and 1% mistagging rate [28,29]. Throughout, a Gaussian smearing of $\Delta\not{E}_T = 20$ GeV is applied to the missing energy vector.

Since most of the signal sensitivity is in the boosted regime $\not{E}_T > 100$ GeV, where the Z-boson decays are produced with small opening angles, we require an extra event selection on their azimuthal angle $\Delta\phi(l, l) < 1.7$. This selection is efficient to further suppress in particular the $t\bar{t}$ and $W(l\nu)Z(ll)$ backgrounds.

Binning in jet multiplicities has been established as an efficient tool to further control the $t\bar{t}$ and other backgrounds. In our analysis, and following standard procedures in similar experimental analyses, the full event sample is divided into zero- and one-jet exclusive subsamples. In Fig. 4, the missing transverse energy distribution, $\not{E}_T$, is depicted for the signal and background components for the zero- (left panel) and one-jet (right panel) exclusive samples. The combination of jet vetoes and large missing energy selections tame both the $Z +$ jets and $t\bar{t}$ backgrounds. Nonetheless, these selections do not result in major extra gains with respect to the VV' background. The structural similarities of this background with respect to the signal, as discussed in Sec. II, result in comparable contributions throughout the whole missing energy distribution profile.

To estimate the 95% C.L. limit to the Higgs to invisible branching ratio $\mathcal{BR}(H \to \text{inv})$, we invoke the CL_s method [30–32]. A two-dimensional binned log-likelihood ratio is used as the test statistic exploring the missing energy distribution $\not{E}_T$ vs the number of jets $n_{\text{jets}} = 0, 1$. This

[2]See the Appendix for further details on the multijet merging for loop-induced processes.

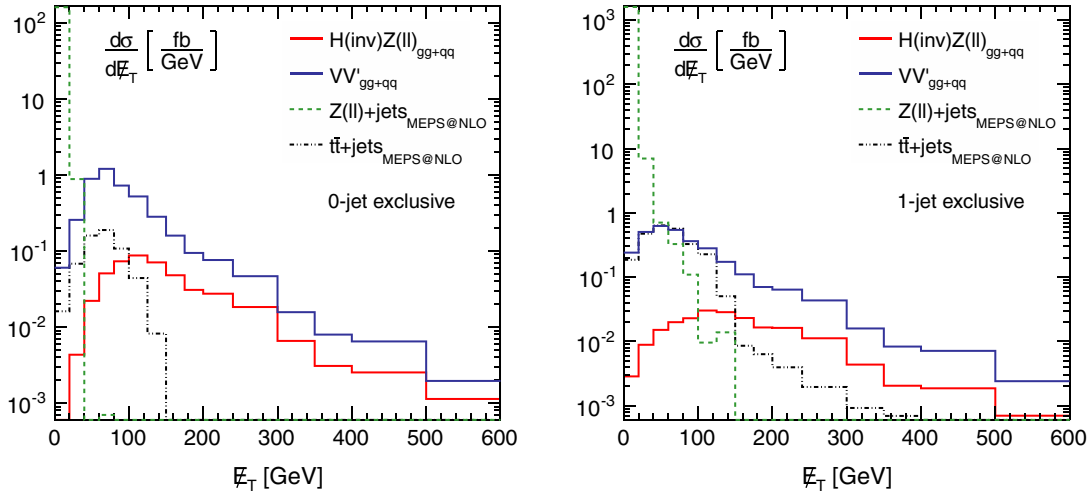

FIG. 4. Missing transverse energy distribution E_T for the signal $H(\text{inv})Z(ll)$ (red) and its major background components $VV' = ZZ, ZW, WW$ (blue), $Z(ll)+\text{jets}$ (green), and $t\bar{t}+\text{jets}$ (black). The zero-jet and one-jet exclusive bin distributions are shown on the left and right, respectively.

procedure scrutinizes the distribution shapes of both panels displayed in Fig. 4. The 95% C.L. upper limit is found by solving $\text{CL}_s(\mu^{95\%})=0.05$, where values $\mathcal{BR}(H\to\text{inv})>\mu^{95\%}$ are excluded at 95% C.L. In Fig. 5 we show the CL_s upper bound to the invisible Higgs boson branching ratio from the Run II LHC. It is possible to bound the branching ratio to $\mathcal{BR}(H\to\text{inv})\lesssim 0.3$ with only 10 fb^{-1} integrated luminosity. To allow a direct appreciation of the importance of the various contributions, in the same figure the resulting bound is also shown, when neglecting separately the GF VV' background and GF HZ: by neglecting the loop-induced background component overly constraining limits would be produced, differing by more than one standard deviation from the correctly expected bound, depending on the luminosity. On the other hand, if the GF signal component was neglected as well, the simulation would present weaker bounds than the more precise prediction that accounts for all the components. At 10 fb^{-1} this would result in shifting the correct bound from $\mathcal{BR}(H\to\text{inv})\lesssim 0.3$ to approximately 0.4.

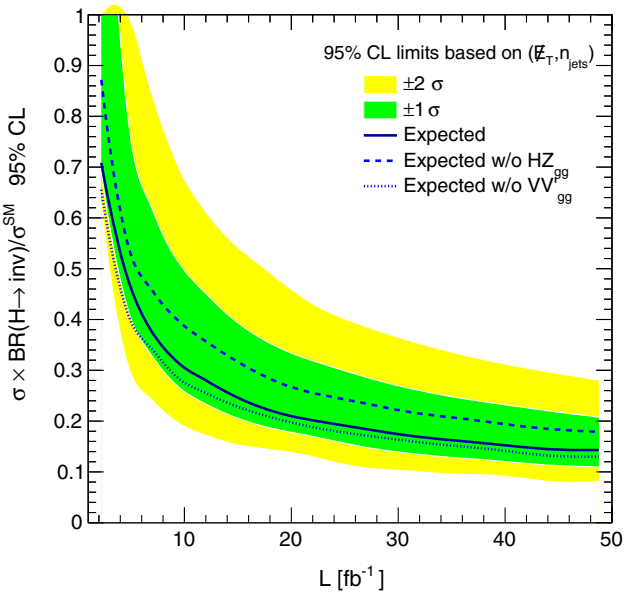

FIG. 5. Expected 95% C.L. upper limit on the $Z(ll)H$ production times the invisible Higgs branching ratio $\mathcal{BR}(H\to\text{inv})$ normalized to the SM production cross section. For comparison, the expected upper limits are also shown when not accounting for the loop-induced $V^{(*)}V'^{(*)}_{gg}$ background (dotted line) and when the loop-induced HZ_{gg} is neglected (dashed line).

It is worth stressing that this analysis provides only an upper bound. Further improvements can be obtained, for instance, by extensive use of multivariate analysis techniques, combining the distributions discussed here with other significant distributions.

IV. CONSTRAINTS ON DARK MATTER SIMPLIFIED MODELS

Searches for beyond the Standard Model (BSM) physics, where the SM degrees of freedom and the new BSM states are separated by a large energy gap, are often performed in an effective field theory (EFT) approach. This is also true for DM searches at the LHC. However, usually these searches require large missing energy selections that render the EFT approach invalid for a significant range of the parameter space [33–40]. Instead of resorting to UV-complete theories, losing the model independency of the derived constraints, a set of *simplified models* was constructed where new particles mediating the interactions between the *visible* and the *dark* sectors [41–47] can be directly produced at colliders. In the present section, we focus on a class of such simplified models with either new scalar or pseudoscalar mediators [48–61].

We assume a Dirac fermion DM χ that can be produced through the decay of either a scalar ϕ or a pseudoscalar A mediator, which are produced by couplings to SM fermions f. We also assume that the interaction respects minimal flavor violation, where the couplings are assumed to be proportional to the Higgs Yukawa interactions. Under these assumptions, flavor constraints are avoided, and the Lagrangian for the interaction terms for the mediator to SM fermions and DM is given by

$$\mathcal{L} \supset -\sum_{\mathrm{f}} \frac{y_f}{\sqrt{2}} (g_v^{\phi} \phi \bar{f} f + i g_v^{A} A \bar{f} \gamma_5 f) - g_{\chi}^{\phi} \phi \bar{\chi} \chi - i g_{\chi}^{A} A \bar{\chi} \gamma_5 \chi, \quad (1)$$

where g_χ is the DM-mediator coupling and g_v is the universal SM fermion-mediator strength.

Such interactions can be probed by multiple channels at the LHC, producing interesting searches for example with missing energy plus top or bottom quarks or jets [48]. Furthermore, the CP nature of the mediator can also be directly probed through spin correlations in the DM production associated with tops [49,62]. Besides these well-studied signatures, the interactions also result in dilepton plus missing energy signatures from the loop-induced $Z(ll)\phi(\chi\chi)$ or $Z(ll)A(\chi\chi)$ channels, with sizable event yields. In the following we derive the complementary LHC bounds that result from these new channels.

In Fig. 6 a representative set of the Feynman diagrams contributing to the DM signal production is shown. While the box-like diagrams only contribute with the Z-boson axial-vector coupling as a consequence of Furry's theorem, the pentagon diagrams can have both vector and axial-vector contributions, allowing particularly Z and photon interference terms. These statements hold for both the scalar and pseudoscalar hypotheses, implying similar total event rates for both scenarios.

The simplified DM signal for the case of a scalar mediator can be obtained in a straightforward way from the GF ZH production in the SM, by simply turning off the HZZ electroweak (EW) coupling, $\kappa_{t,V} = (1, 0)$. For comparison, the $pp \to Z(ll)H(\mathrm{inv})$ is decomposed in Fig. 7 into a DY and a $\mathrm{GF}_{\kappa_{t,V}=(1,1)}$ component, as discussed in some detail in the previous sections. The GF is further decomposed by separately switching off the fermion couplings, $\mathrm{GF}_{\kappa_{t,V}=(0,1)}$,

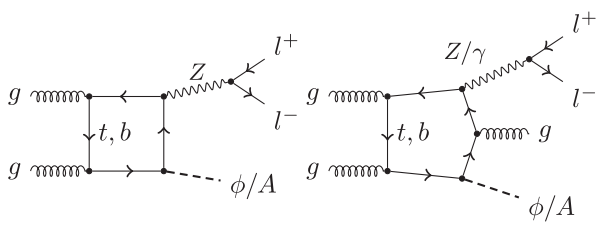

FIG. 6. Representative loop-induced Feynman diagrams contributing to the signals $l^+l^-\phi/A$ (left) and $l^+l^-\phi/Aj$ (right).

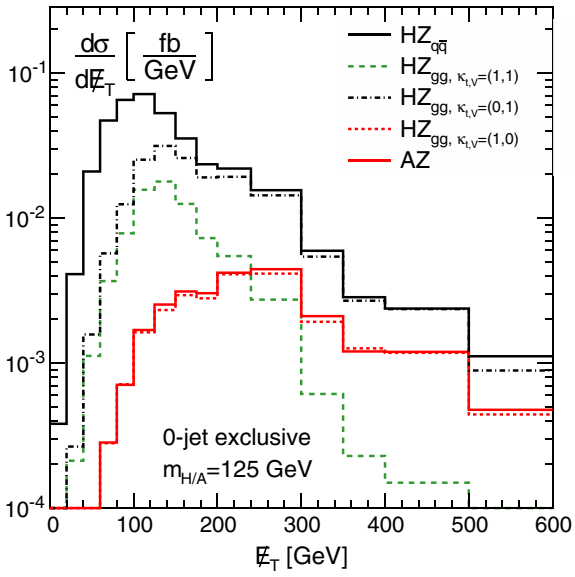

FIG. 7. Transverse missing energy distribution E_T for $pp \to Z(ll)H(\mathrm{inv})$. The following components are shown: DY (black full), GF (green dashed), GF with the scalar-vector boson interactions switched off $\kappa_{t,V} = (1, 0)$ (red dashed), and GF with the Yukawa interactions switched off $\kappa_{t,V} = (0, 1)$ (black dot-dashed). Notice that the GF curve with $\kappa_{t,V} = (1, 0)$ corresponds to our scalar simplified model. For comparison, the pseudoscalar channel $pp \to Z(ll)A(\mathrm{inv})$ (red full) is also added. In this plot $m_{H/A} = 125$ GeV and $\mathcal{BR}(H/A \to \mathrm{inv}) = 1$. The DY and GF samples are merged up to one jet, respectively, with MEPS@NLO and MEPS@LOOP^2 technology.

and the EW couplings, $\mathrm{GF}_{\kappa_{t,V}=(1,0)}$. The latter, $\mathrm{GF}_{\kappa_{t,V}=(1,0)}$ (i.e., the scalar DM simplified model), presents enhanced rates in the boosted regime that are comparable to the DY component. To inspect differences between scenarios with scalar and pseudoscalar mediators, the $\not{E}_T$ distribution in $pp \to Z(ll)A(\mathrm{inv})$ is also added. It is very similar in both rate and shape to the loop-induced $Z(ll)H(\mathrm{inv})$ contribution, differing by less than 10% over the full missing energy distribution.

We reproduce the analysis strategy presented in the previous section and perform a two-dimensional binned log-likelihood analysis based on the $\not{E}_T$ and n_{jets} distributions. In Fig. 8, the expected 95% C.L. upper limit on the mediator coupling to fermions g_v is depicted as a function of the mediator mass $m_{\phi/A}$ for scalars (left) and pseudoscalars (right). Assuming 100 fb^{-1} of data and $\mathcal{BR}(\phi/A \to \chi\chi) = 1$, we can bound the signal over the full considered mass range 100 GeV $< m_{\phi/A} <$ 400 GeV to $g_v < 1$. Furthermore, the bounds for the two simplified models are very similar as a result of their comparable distribution profiles which differ by only a few percent. Figure 8 also shows the 95% C.L. noncollider experimental bounds for DM direct and indirect detection, as well as for thermal relic abundance cross section bounds [48,49]. While the pseudoscalar mediator does not induce

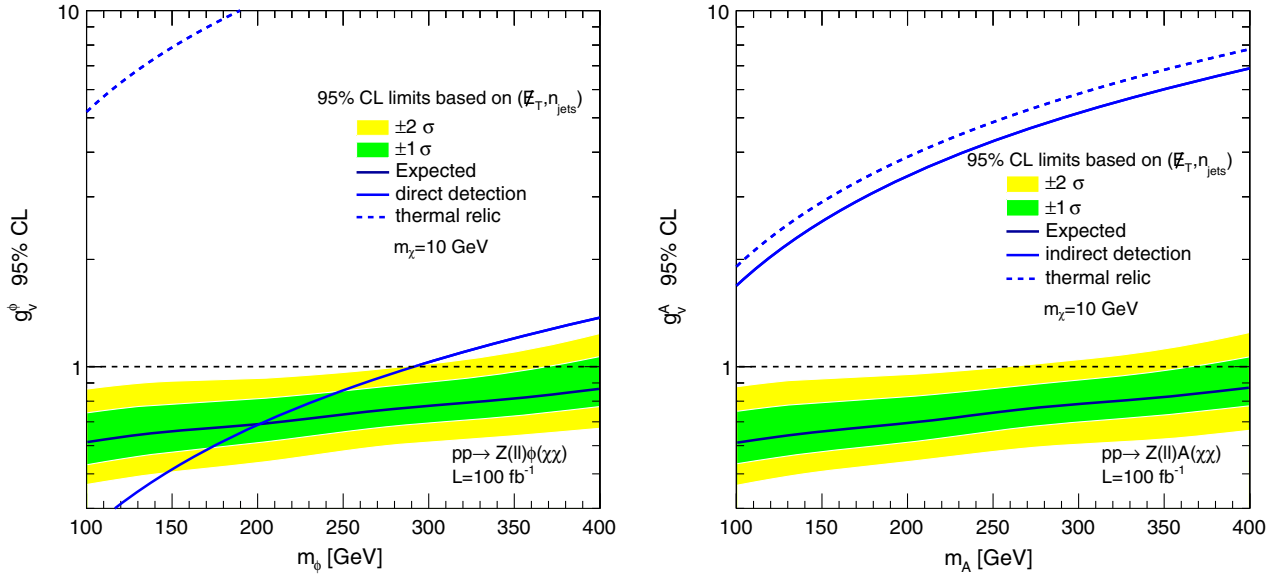

FIG. 8. Expected 95% C.L. upper limit on the mediator coupling to fermions g_v as a function of the mediator mass $m_{\phi/A}$ for scalars (left) and pseudoscalars (right). The binned log-likelihood test is based on the two-dimensional distributions (E_T, n_{jets}) for 100 fb^{-1} of LHC data assuming $\mathcal{BR}(\phi/A \to \chi\chi) = 1$. In addition, the 95% C.L. upper limits on scalar mediators from LUX direct detection bounds [63] and on pseudoscalars from the Fermi-LAT dwarf galaxy search [65] are included. The required g_v value for the thermal relic is also shown in both cases.

a momentum-independent scattering cross section with nuclei, and so does not display relevant limits from direct detection experiments, the scalar mediator scenario generates a spin-independent rate resulting in strong bounds from several experiments. The most stringent ones come from LUX [63] for large DM masses $m_\chi > 6$ GeV and from CDMSLite [64] for lower DM masses. The indirect detection bounds are obtained from the $b\bar{b}$ channel using the Fermi Large Area Telescope data on dwarf galaxies [65]. This bound is only relevant to the pseudoscalar mediators because scalar mediators present velocity-suppressed thermal cross sections and DM in the present Universe is moving much slower than the speed of light ($T \ll m_\chi$). Last, both mediator models display relevant bounds from the thermal relic abundance, assuming $\langle\sigma v\rangle = 3 \times 10^{-26}$ cm^3/s in the early Universe and $g_v = g_\chi$ to make the comparisons to collider bounds more straightforward. Under the presented assumptions, the LHC can provide stronger constraints than the noncollider limits for almost the entire considered mediator mass region. It only presents weaker constraints for lower scalar mediator masses $m_\phi < 200$ GeV, where the direct detection bounds are more relevant. Importantly, pseudoscalar mediator scenarios are much more challenging for noncollider experiments and the LHC bounds become even more important.

It must be stressed at this point, however, that no single result quoted here, from collider and noncollider experiments, should be taken as the final word. The analyses discussed here approach the same problem from different angles and with different assumptions. For instance, these bounds can be significantly changed if more particles are present in the spectrum beyond our benchmark scenario. In this sense, the presented limits should be seen more as a guide that allows us to focus on particular parameter-space regions with the correspondent experimental data.

V. SUMMARY

In this paper a state of the art analysis for the searches for invisible decays of Higgs bosons in their Z-associated production channel has been performed, focusing on $\ell\ell + \not{E}_T$ final states. The importance of the loop-induced contributions to both the signal $Z(ll)H(\text{inv})$ and the backgrounds WW and ZZ has been discussed in detail for the first time, taking into account the effect of multijet merging technology. Both contributions lead to relevant changes in important distributions and therefore effects in the CL$_s$ bounds that can go beyond the 1σ uncertainty, depending on the collider luminosity.

The two-dimensional $(\not{E}_T, n_{\text{jets}})$ binned log-likelihood analysis in particular shows that the invisible Higgs branching ratio can be bound to $\mathcal{BR}(H \to \text{inv}) < 0.15$ with $\mathcal{L} = 50$ fb^{-1} of data at the LHC 13 TeV. In our analysis we confirmed that the separation into zero- and one-jet bins is fundamental to maximize the control over the otherwise dominant background $t\bar{t}$ + jets. We also showed that multijet merging techniques are fundamental for this analysis, and especially when performing the separation into jet bins.

We extended the analysis to a set of simplified models of dark matter which connect the visible and invisible sectors through scalar or pseudoscalar mediators. We found that the $Z\phi(A)$ channel provides relevant bounds to this type of models being able to probe the mediator masses in the range of 100 GeV $< m_{\phi/A} = 400$ GeV with 100 fb^{-1}.

APPENDIX: MERGING FOR LOOP-INDUCED PROCESSES: VALIDATION

In Fig. 4 (right panel), we illustrate how matrix element corrections included through the merging algorithm significantly affect the transverse momentum spectrum for high-energy jets, $p_T^{j_{\text{lead}}} > 100$ GeV. This is an expected feature since the parton shower cannot appropriately fill phase-space regions where the jet transverse momentum significantly exceeds the mass of the produced electroweak final state. Therefore, we observe a strong enhancement in the $p_T^{j_{\text{lead}}}$ tail for both the signal and the background processes when employing multijet merging.

However, for the background, this enhancement does not result in an enhancement for the E_T^{miss} distribution. Since a high-p_T jet must, to some degree, recoil against the neutrinos in this process, the lack of an enhancement in the E_T^{miss} distribution is rather surprising. It can, however, be attributed to two circumstances. First, the relative contributions at the E_T^{miss} tail from large $p_T^{j_{\text{lead}}}$ configurations are moderate. This is explicitly shown in Fig. 9 (top), where we plot those contributions and compare their relative impact on the inclusive spectrum. Second, although there is an enhancement at high-$p_T^{j_{\text{lead}}}$ events when employing multijet merging, there is also a suppression in the intermediate $p_T^{j_{\text{lead}}}$ regime. In Fig. 9 (bottom), we observe that this suppression factor reaches almost 0.5 at $p_T^{j_{\text{lead}}} \approx 50$ GeV. The corresponding phase space does, to some extent, overlap with the high-E_T^{miss} region and therefore compensates an enhancement in this region that would be due to large $p_T^{j_{\text{lead}}}$ configurations.

In order to demonstrate that the suppression of the intermediate $p_T^{j_{\text{lead}}}$ region is a genuine effect of the higher-multiplicity processes that we include through merging, we compare our results for the leading jet transverse momentum spectrum to a fixed-order calculation in the bottom panel of Fig. 9. We observe a very good agreement of the fixed-order results with the multijet merged prediction in the relevant regions of phase space recovering the suppression around $p_T^{j_{\text{lead}}} \approx 50$ GeV.

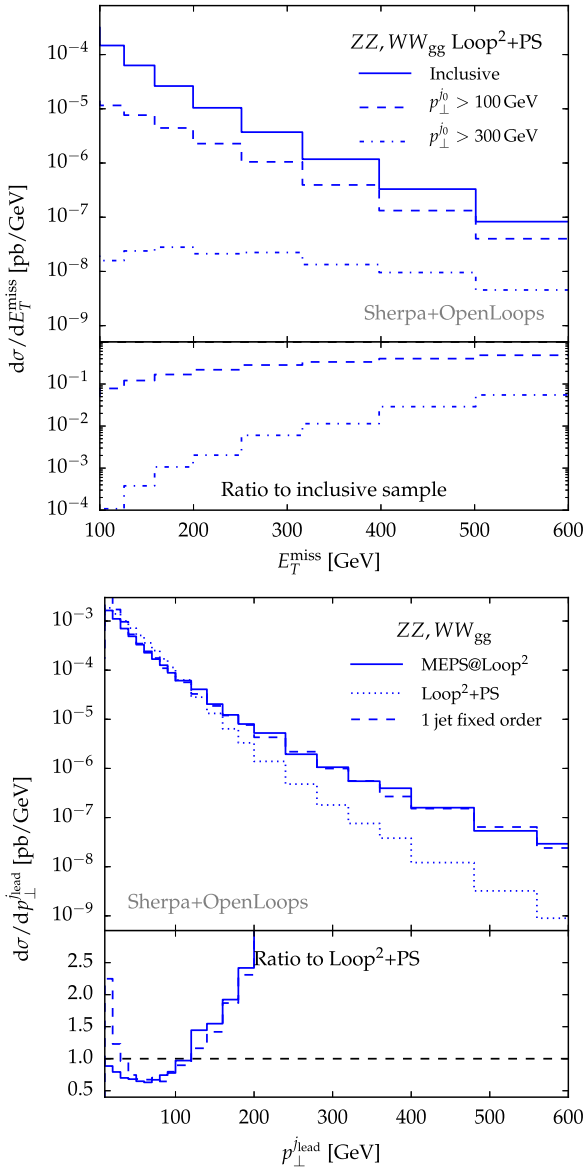

FIG. 9. Transverse missing energy E_T^{miss} distribution (top) and leading jet transverse momentum $p_T^{j_{\text{lead}}}$ spectra (bottom) for the loop-induced component of the ZZ, WW process. In the bottom panel, we compare the fixed-order $(ZZj, WWj)_{gg}$ result to the prediction obtained from a multijet merging setup.

[1] P. W. Higgs, Phys. Lett. **12**, 132 (1964); Phys. Rev. Lett. **13**, 508 (1964); Phys. Rev. **145**, 1156 (1966); F. Englert and R. Brout, Phys. Rev. Lett. **13**, 321 (1964); G. S. Guralnik, C. R. Hagen, and T. W. Kibble, Phys. Rev. Lett. **13**, 585 (1964).

[2] G. Aad *et al.* (ATLAS Collaboration), Phys. Lett. B **716**, 1 (2012); S. Chatrchyan *et al.* (CMS Collaboration), Phys. Lett. B **716**, 30 (2012).

[3] G. Aad *et al.* (ATLAS Collaboration), Phys. Rev. Lett. **112**, 201802 (2014); S. Chatrchyan *et al.* (CMS Collaboration), Eur. Phys. J. C **74**, 2980 (2014).

[4] T. Corbett, O. J. P. Eboli, D. Goncalves, J. Gonzalez-Fraile, T. Plehn, and M. Rauch, J. High Energy Phys. 08 (2015) 156.

[5] R. M. Godbole, M. Guchait, K. Mazumdar, S. Moretti, and D. P. Roy, Phys. Lett. B **571**, 184 (2003); D. Ghosh, R. Godbole, M. Guchait, K. Mohan, and D. Sengupta, Phys. Lett. B **725**, 344 (2013).

[6] O. J. P. Eboli and D. Zeppenfeld, Phys. Lett. B **495**, 147 (2000).

[7] A. Dedes, T. Figy, S. Hoche, F. Krauss, and T. E. J. Underwood, J. High Energy Phys. 11 (2008) 036; C. Englert, T. Plehn, D. Zerwas, and P. M. Zerwas, Phys. Lett. B **703**, 298 (2011).

[8] C. Bernaciak, T. Plehn, P. Schichtel, and J. Tattersall, Phys. Rev. D **91**, 035024 (2015).

[9] D. Goncalves, F. Krauss, S. Kuttimalai, and P. Maierhfer, Phys. Rev. D **92**, 073006 (2015).

[10] L. Altenkamp, S. Dittmaier, R. V. Harlander, H. Rzehak, and T. J. E. Zirke, J. High Energy Phys. 02 (2013) 078; C. Englert, M. McCullough, and M. Spannowsky, Phys. Rev. D **89**, 013013 (2014).

[11] G. Luisoni, P. Nason, C. Oleari, and F. Tramontano, J. High Energy Phys. 10 (2013) 083; S. Hoeche, F. Krauss, S. Pozzorini, M. Schoenherr, J. M. Thompson, and K. C. Zapp, Phys. Rev. D **89**, 093015 (2014).

[12] B. Hespel, F. Maltoni, and E. Vryonidou, J. High Energy Phys. 06 (2015) 065.

[13] O. Brein, A. Djouadi, and R. Harlander, Phys. Lett. B **579**, 149 (2004).

[14] M. L. Ciccolini, S. Dittmaier, and M. Kramer, Phys. Rev. D **68**, 073003 (2003).

[15] O. Brein, R. Harlander, M. Wiesemann, and T. Zirke, Eur. Phys. J. C **72**, 1868 (2012).

[16] L. Altenkamp, S. Dittmaier, R. V. Harlander, H. Rzehak, and T. J. E. Zirke, J. High Energy Phys. 02 (2013) 078.

[17] F. Cascioli, S. Höche, F. Krauss, P. Maierhöfer, S. Pozzorini, and F. Siegert, J. High Energy Phys. 01 (2014) 046.

[18] S. Höche, F. Krauss, M. Schönherr, and F. Siegert, J. High Energy Phys. 04 (2013) 027; T. Gehrmann, S. Höche, F. Krauss, M. Schönherr, and F. Siegert, J. High Energy Phys. 01 (2013) 144.

[19] S. Frixione and B. R. Webber, J. High Energy Phys. 06 (2002) 029.

[20] S. Höche, F. Krauss, M. Schönherr, and F. Siegert, J. High Energy Phys. 09 (2012) 049; Phys. Rev. Lett. **110**, 052001 (2013).

[21] S. Catani, F. Krauss, R. Kuhn, and B. R. Webber, J. High Energy Phys. 11 (2001) 063; F. Krauss, J. High Energy Phys. 08 (2002) 015; S. Hoeche, F. Krauss, S. Schumann, and F. Siegert, J. High Energy Phys. 05 (2009) 053.

[22] M. Buschmann, D. Goncalves, S. Kuttimalai, M. Schonherr, F. Krauss, and T. Plehn, J. High Energy Phys. 02 (2015) 038.

[23] M. Buschmann, C. Englert, D. Goncalves, T. Plehn, and M. Spannowsky, Phys. Rev. D **90**, 013010 (2014).

[24] T. Gleisberg, S. Höche, F. Krauss, M. Schönherr, S. Schumann, F. Siegert, and J. Winter, J. High Energy Phys. 02 (2009) 007.

[25] F. Cascioli, P. Maierhöfer, and S. Pozzorini, Phys. Rev. Lett. **108**, 111601 (2012).

[26] A. Denner, S. Dittmaier, and L. Hofer, arXiv:1604.06792.

[27] M. Cacciari, G. P. Salam, and G. Soyez, J. High Energy Phys. 04 (2008) 063; Eur. Phys. J. C **72**, 1896 (2012).

[28] CMS Collaboration, Report No. CMS-PAS-BTV-13-001.

[29] D. Goncalves, F. Krauss, and R. Linten, Phys. Rev. D **93**, 053013 (2016).

[30] J. Neyman and E. S. Pearson, Phil. Trans. R. Soc. A **231**, 289 (1933).

[31] A. L. Read, J. Phys. G **28**, 2693 (2002).

[32] T. Junk, Nucl. Instrum. Methods Phys. Res., Sect. A **434**, 435 (1999).

[33] P. J. Fox, R. Harnik, J. Kopp, and Y. Tsai, Phys. Rev. D **84**, 014028 (2011).

[34] I. M. Shoemaker and L. Vecchi, Phys. Rev. D **86**, 015023 (2012).

[35] N. Weiner and I. Yavin, Phys. Rev. D **86**, 075021 (2012).

[36] G. Busoni, A. De Simone, E. Morgante, and A. Riotto, Phys. Lett. B **728**, 412 (2014).

[37] O. Buchmueller, M. J. Dolan, and C. McCabe, J. High Energy Phys. 01 (2014) 025.

[38] O. Buchmueller, M. J. Dolan, S. A. Malik, and C. McCabe, J. High Energy Phys. 01 (2015) 037.

[39] G. Busoni, A. De Simone, J. Gramling, E. Morgante, and A. Riotto, J. Cosmol. Astropart. Phys. 06 (2014) 060.

[40] G. Busoni, A. De Simone, T. Jacques, E. Morgante, and A. Riotto, J. Cosmol. Astropart. Phys. 09 (2014) 022.

[41] J. Alwall, P. Schuster, and N. Toro, Phys. Rev. D **79**, 075020 (2009).

[42] D. Alves *et al.* (LHC New Physics Working Group Collaboration), J. Phys. G **39**, 105005 (2012).

[43] J. Goodman and W. Shepherd, arXiv:1111.2359.

[44] T. Jacques and K. Nordstrm, J. High Energy Phys. 06 (2015) 142.

[45] R. M. Godbole, G. Mendiratta, and T. M. P. Tait, J. High Energy Phys. 08 (2015) 064.

[46] J. Abdallah *et al.*, Phys. Dark Univ. **9–10**, 8 (2015).

[47] D. Abercrombie *et al.*, arXiv:1507.00966.

[48] M. R. Buckley, D. Feld, and D. Goncalves, Phys. Rev. D **91**, 015017 (2015).

[49] M. R. Buckley and D. Goncalves, Phys. Rev. D **93**, 034003 (2016).

[50] U. Haisch, F. Kahlhoefer, and J. Unwin, J. High Energy Phys. 07 (2013) 125.

[51] U. Haisch, F. Kahlhoefer, and E. Re, J. High Energy Phys. 12 (2013) 007.

[52] U. Haisch, A. Hibbs, and E. Re, Phys. Rev. D **89**, 034009 (2014).
[53] A. Crivellin, F. D'Eramo, and M. Procura, Phys. Rev. Lett. **112**, 191304 (2014).
[54] K. Ghorbani, J. Cosmol. Astropart. Phys. 01 (2015) 015.
[55] C. Englert, M. McCullough, and M. Spannowsky, arXiv: 1604.07975.
[56] S. Baek, P. Ko, M. Park, W. I. Park, and C. Yu, Phys. Lett. B **756**, 289 (2016).
[57] M. Backovi, M. Kramer, F. Maltoni, A. Martini, K. Mawatari, and M. Pellen, Eur. Phys. J. C **75**, 482 (2015).
[58] P. Harris, V. V. Khoze, M. Spannowsky, and C. Williams, Phys. Rev. D **91**, 055009 (2015).
[59] O. Mattelaer and E. Vryonidou, Eur. Phys. J. C **75**, 436 (2015).
[60] U. Haisch and E. Re, J. High Energy Phys. 06 (2015) 078.
[61] A. Berlin, S. Gori, T. Lin, and L. T. Wang, Phys. Rev. D **92**, 015005 (2015).
[62] M. R. Buckley and D. Goncalves, Phys. Rev. Lett. **116**, 091801 (2016).
[63] D. S. Akerib *et al.* (LUX Collaboration), Phys. Rev. Lett. **112**, 091303 (2014).
[64] R. Agnese *et al.* (SuperCDMS Collaboration), Phys. Rev. Lett. **112**, 041302 (2014).
[65] M. Ackermann *et al.* (Fermi-LAT Collaboration), Phys. Rev. Lett. **115**, 231301 (2015).